The Dynamics of Thin Liquid Films in the Presence of Surface-Tension Gradients

V. LUDVIKSSON
and
E. N. LIGHTFOOT
University of Wisconsin, Madison, Wisconsin

The climbing of Marangoni films up vertical solid surfaces was investigated experimentally and theoretically. The system considered was a nonisothermal plate with its warm end partially immersed in a nonvolatile liquid. Observed film thicknesses and rates of climb were in agreement with an approximate hydrodynamic model obtained by assuming the supply capacity of the film to be rate limiting.

The results of this study confirm the hypothesis that previously observed liquid films formed against gravitational forces above equilibrium menisci are produced by surface-tension inequalities. It is pointed out that hydrodynamic processes cannot allow for the advancement of the leading edge of Marangoni films and a separate physicochemical process is required to explain spontaneous spreading of these films. Evidence is presented for the formation of much thinner primary films ahead of the secondary bulk films described by hydrodynamics. These primary films appear to be produced by a combination of multilayer adsorption and/or surface diffusion. The kinetics of these diffusional processes may limit spreading rates when surface-tension gradients become sufficiently large.

Finally, the Marangoni films were found to be unstable in a manner hitherto not considered.

The tendency for thin films of liquids to rise above the equilibrium meniscus on inclined wetted solid surfaces has been demonstrated for both aqueous electrolytes (*13*) and organic liquids (*1*). The formation of such "super-meniscus" films has been shown to be important in the operation of gas-diffusion electrodes by Will (*21*) and in boundary lubrication by Bascom, Cottington, and Singleterry (*1*). Similar films may occur in many other situations of importance such as evaporation and boiling of liquids, condensation of vapors, and perhaps the movement of water in oil fields. The existence of these films and their ability to spread against the pull of gravity have been attributed qualitatively to the presence of upward directed surface-tension gradients (*1*). In this paper we provide quantitative experimental confirmation of this hypothesis and review briefly the hydrodynamic aspects of spontaneous spreading.

Interpretation of the experimental data is based on an extension of a previously described (*8*) approximate solution of the "film" equations of motion which is purely hydrodynamic in nature. As we have already pointed out (*10*), such an analysis cannot describe advancement of the film front in detail, and we are therefore forced to make rather crude approximations in the frontal region. It is hoped that the film profiles presented in this paper, along with similar data now being gathered in capillary rise experiments, will lead to an improved understanding of this region. It will, however, be shown that many of the important characteristics of surface-tension driven flows can be satisfactorily described on the basis of our present development.

THEORY

Local Description of Marangoni Films

The system we consider is a thin liquid film advancing up a flat vertical surface under the influence of an upwardly directed surface-tension gradient γ, as shown in Figure 1. We assume the fluid velocity to be small and the film thin so that we can neglect fluid inertia and consider the flow to be locally one-dimensional. For these conditions it is also possible to neglect transfer of momentum in the direction of flow.

The equations of motion for any segment of the film can then be written as

$$-\frac{\partial p}{\partial z}+\mu\frac{\partial^2 v_z}{\partial y^2}+\rho g_z=0 \tag{1}$$

and

$$\frac{\partial p}{\partial y}=0 \tag{2}$$

Since p is not a function of y we are able to integrate Equation (1) locally with the aid of the boundary conditions

$$\text{B.C. 1} \quad \text{at} \quad y=0 \quad v_z=0 \tag{3}$$

that is, no slip at the solid, and

$$\text{B.C. 2} \quad \text{at} \quad y=h \quad \mu\frac{\partial v_z}{\partial y}=\gamma \tag{4}$$

Note that for the coordinate system chosen $g_z=-g$. The velocity profile corresponding to this description is

$$v_z=\frac{1}{\mu}\left(\frac{\partial p}{\partial z}+\rho g\right)\left(\frac{1}{2}y^2-hy\right)+\frac{\gamma y}{\mu} \tag{5}$$

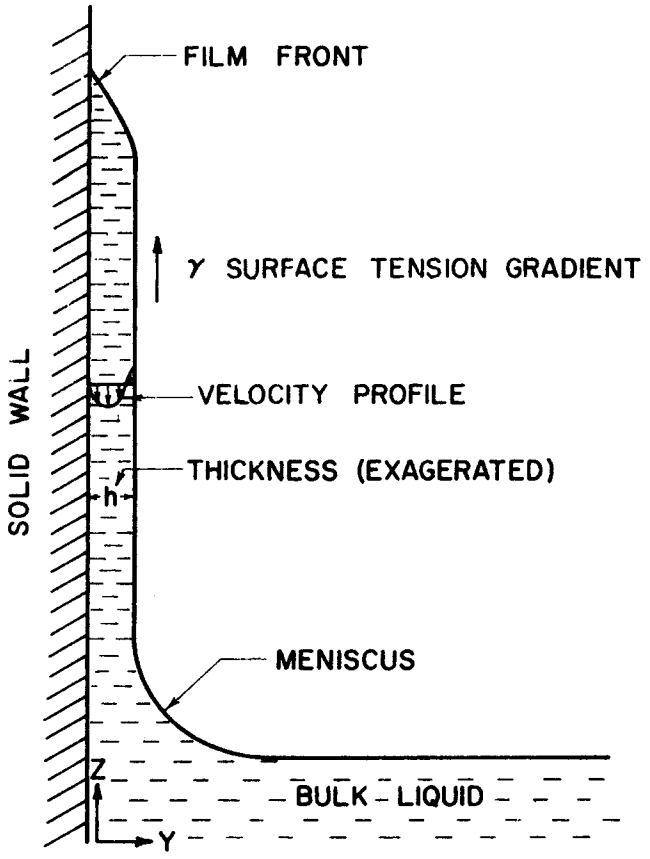

Fig. 1. Generalized picture of flow in thin liquid films.

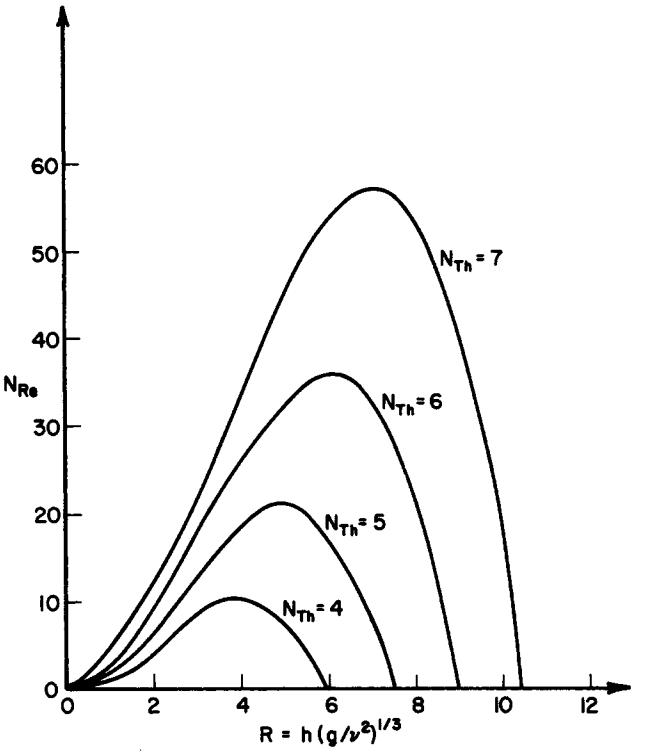

Fig. 2. Effect of Thomson number on film flow rate.

The local average flow rate is

$$v_z\rangle = -\frac{1}{\mu}\left(\frac{\partial p}{\partial z} + \rho g\right)\frac{h^2}{3} + \frac{\gamma h}{2\mu} \tag{6}$$

Thus we see that the net flow can be upward, downward, or zero, depending on the relative magnitude of the terms in Equation (6).

Equations (5) and (6) describe the local flow behavior of a large number of film problems in draining and spreading. Tallmadge and Gutfinger (*18*) have recently reviewed a number of systems in which surface-tension gradients are not expected so that the last term of the above equation disappears.

It should be noted that the term $\partial p/\partial z$ depends on the film shape and that without further constraints we cannot determine the velocity or the film thickness uniquely. However, it will be shown in the experimental section that for many experimental conditions $\partial p/\partial z \ll \rho g$, so that the film can be considered locally flat. For this situation we can write Equation (6) in the simplified dimensionless form

$$N_{Re} = \frac{1}{2} R^2 N_{Th} - \frac{1}{3} R^3 \tag{7}$$

This Reynolds number-film thickness relation is plotted in Figure 2. For positive Thomson numbers,* there is clearly a flow maximum of

$$N_{Re_{max}} = \frac{1}{6} N_{Th}^3 \tag{8}$$

*We previously called this group the Marangoni number (*8*) but have since (*12*) adopted the convention used by Pearson (*16*) and Scriven and Sternling (*17*) for the Marangoni number. Instead we rename this group for the man who first correctly explained the effects of surface-tension gradients (Marangoni effects), J. J. Thomson (*19*).

for a dimensionless film thickness given by

$$R = N_{Th} \tag{9}$$

There are also two film thicknesses yielding no flow: $R = 0$ and $R = \frac{3}{2}N_{Th}$. An experimental test of these results is reported below. A mathematical investigation of possible instabilities resulting from the double-valued nature of Equation (7) is in progress.

Formal Analysis of Film Growth

To obtain a differential equation describing the growth of a spreading film, we begin with a macroscopic mass balance in the form

$$\frac{\partial h}{\partial t} = -\frac{\partial}{\partial z}\langle v_z\rangle h \tag{10}$$

Insertion of Equation (6) into this expression yields

$$\frac{\partial h}{\partial t} = \frac{\partial}{\partial z}\left[\frac{1}{\mu}\left(\frac{\partial p}{\partial z} + \rho g\right)\frac{h^3}{3} - \frac{\gamma h^2}{2\mu}\right] \tag{11}$$

which provides the needed relation for $h(z, t)$. To complete the description of film dynamics it remains only to relate the pressure gradient to surface curvature and to specify a suitable set of boundary conditions. Expressions for curvature pressure are readily available (*6,7*), but specification of boundary conditions is as yet very difficult.

The primary difficulty in application of Equation (11) is that this expression is incapable of describing flow conditions at the interline between the advancing meniscus and the as yet unwetted surface immediately beyond it. This can be seen by noting that $\partial h/\partial t$ is zero when h is zero. This situation arises from the postulate of zero slip velocity between the liquid and the solid wall surface, Equation (3), and not from any of the simplifications introduced into the equations of motion. It therefore follows, as we have already pointed out (*10*), that the spreading of liquids

cannot be explained solely on a hydrodynamic basis. Rather the edge of the meniscus must advance by a diffusional process which is most probably made possible by multilayer adsorption in a very thin primary film formed ahead of the meniscus. Qualitative visual evidence for very thin primary films has been obtained by various investigators (*1, 5, 13*) and by us during the course of this work, as indicated below. Such films have also been discussed in connection with flow through porous media (*2, 3*).

One can integrate Equation (11) and obtain a plausible model description of spreading by postulating the presence of such a preformed primary film; that is, we can postulate that the film never is thinner than the primary film. Descriptions based on this postulate appear to be consistent with available experimental measurements for the rise of liquids in capillary tubes (*10*), and we are currently investigating the usefulness of this approach. At present, however, one cannot describe conditions at the advancing meniscus front with any confidence. It is therefore preferable to postpone detailed consideration of this region and to use a simplified approach. One method of doing this is outlined in the next section.

Preliminary Treatment of Spreading

In this section we assume that film spreading over a wettable surface is determined primarily by the supply ("pumping") capacity of the film and not by the specific conditions in the curved region near the advancing edge of the meniscus. We further postulate that the inventory of liquid in this curved region is sufficiently small that it may be considered constant. We may therefore ignore both curvature pressure and the poorly understood diffusional processes taking place at the edge of the meniscus.

By neglecting curvature we may simplify Equation (11) and write it in dimensionless form as

$$\frac{\partial R}{\partial \tau} = -(RN_{Th} - R^2)\,\frac{\partial R}{\partial Z} \tag{12}$$

For convenience we assume that the film height is initially zero for $R \geq 0$. We may therefore integrate Equation (13) to obtain

$$Z = (RN_{Th} - R^2)\,\tau \tag{13}$$

following the positions of any constant R. Equation (13) is used in Figure 3 to show calculated film shapes (after dividing through by N_{Th}^2) for several times (solid lines). It is seen immediately that the calculated R is a double-valued function of position. This is a physically meaningless result obtained by neglect of surface curvature. Analogous multiple-valued profiles are obtained for concentration waves in fixed sorbent beds when solute dispersion is neglected (*4, 9*) and for shallow-water waves if viscous dissipation is not taken into consideration.

Just as in these analogous situations a useful asymptotic result can be obtained by replacing the double-valued front by a combination of sharp (or discontinuous) and diffuse portions satisfying the same mass balance. Such asymptotic fronts are represented in Figure 3 for $\tau = 1$ and $\tau = 2$ by heavy dotted lines. The position Z_d of the sharp portion of the front, and the film thickness R_d where it meets the diffuse portion, are determined for our boundary conditions by means of the mass-balance relation:

$$\frac{1}{2}R_{\max}N_{Th} - \frac{1}{3}R_{\max}^3 = \left(\frac{Z_d}{\tau}\right)R_d + \int_{R_d}^{R_{\max}}\left(\frac{\partial Z}{\partial \tau}\right)_R dR \tag{14}$$

Here $R_{\max}$ is the limiting thickness as $\tau \longrightarrow \infty$. It is given by $R_{\max} = N_{Th}$ by Equation (6). This is also the thickness of maximum flow rate as given by Equation (9). Using Equation (13) and performing the integration in Equation

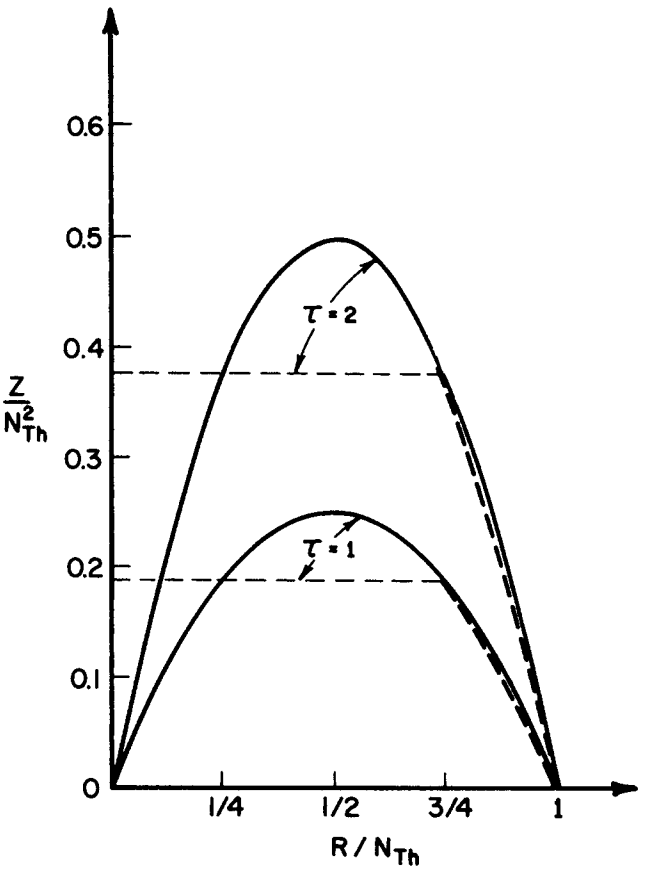

Fig. 3. Approximate climbing characteristics of liquid films.

(14), we get an equation for R_d

$$\frac{1}{2}N_{Th}^3 - \frac{1}{3}N_{Th}^3 = (R_d^2 N_{Th} - R_d^3) + \left[\frac{1}{2}R^2 N_{Th} - \frac{1}{3}R^3\right]\frac{N_{Th}}{R_d} \tag{15}$$

so that

$$R_d = \frac{3}{4}N_{Th} \tag{16}$$

$$Z_d = \frac{3}{16}N_{Th}^2 \tag{17}$$

Thus we find that the film climbs at a steady rate expressed by Equation (17) and that the advancing front is three-quarters as wide as the steady state film corresponding to maximum flow rate [see Equation (9)]. The dimensionless speed $\frac{dZ_d}{d\tau} = \frac{3}{16}N_{Th}^2$ at which this front advances is just slightly in excess of the dimensionless average velocity $N_{Re_{\max}}/R_{\max} = \frac{1}{6}N_{Th}^2$ of the steady film at maximum flow. However, it is also important to note, as seen from Equation (15), that the final thickness of the climbing film $R_{\max} = N_{Th}$ is only approached asymptotically for $\tau/Z \longrightarrow \infty$.

Equations (15) through (18) will be valid only if conditions in the frontal region (primary film) permit the predicted rate of spreading and if inventory changes in the frontal region are unimportant. It appears reasonable on physical grounds that such a condition should be approached for large time, as is the case for the previously mentioned concentration and shallow-water waves. This has not yet been demonstrated, however, and the utility of these equations is yet to be determined in detail. As we shall see they are in substantial agreement with our experimental results.

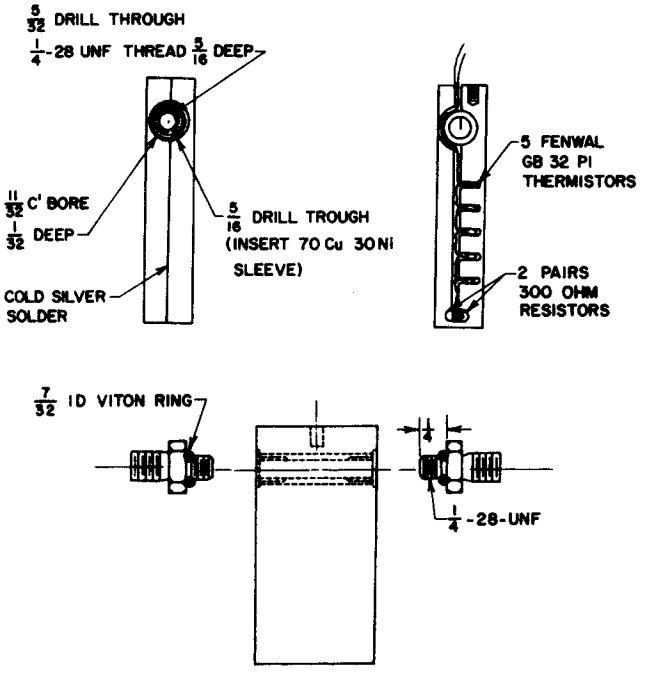

Fig. 4a. Temperature-controlled plate assembly.

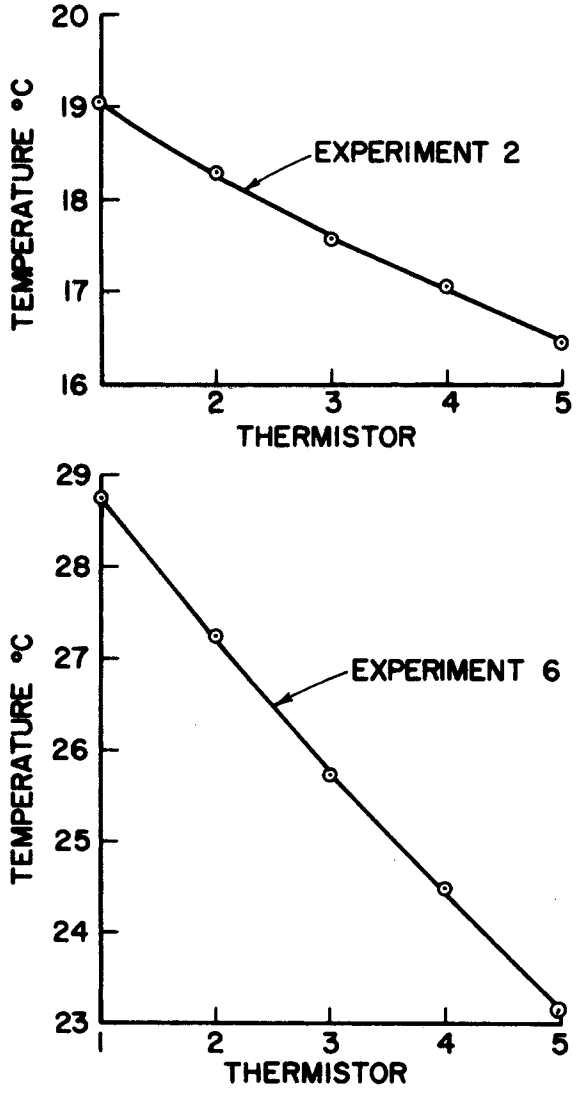

Fig. 4b. Sample temperature profiles in silver plate.

EXPERIMENT

The purpose of the experimental part of the program was to make quantitative observations of film spreading under the conditions considered from a mathematical standpoint in the previous section. These observations serve as a means of testing the approximate theory just discussed and as preparation for a more detailed analysis.

Techniques

It was decided to build directly upon the earlier work of Bascom et al. (*1*) and hence to study the climbing of squalane films on vertical metal surfaces. However, we felt it would be preferable to produce surface-tension gradients by maintaining a known temperature gradient in the film rather than to depend upon the development of concentration gradients via selective evaporation. Much more effective control of surface-tension gradients can be maintained in this way, and interpretation of the experimental observations is both simpler and less ambiguous. We therefore used as the solid phase a polished silver plate cooled at the top by means of an imbedded water-cooled tube and heated at the bottom by imbedded resistors. Film profiles were determined by an interferometric method previously described elsewhere (*1*, *11*, *13* to *15*), and shown schematically in Figure 5.

The test plate used in these experiments is described schematically in Figure 4. It consists of two ($1\frac{1}{4}$ in. $\times$ $2\frac{1}{2}$ in.) silver plates silver-soldered together and containing imbedded heating elements, five thermistors $\frac{1}{4}$ in. apart, and a cooling tube as shown. Cold silver solder was used to join the plates to avoid any nonmetallic surface elements which might contaminate the thin films studied, and at the same time to avoid thermal damage to the thermistors and resistors. The plate was constructed of silver because prior calculations (*11*) showed that a high thermal conductivity was desirable for maintenance of a constant temperature gradient over the plate surface. It was shown that for the test plate used temperature gradients were constant to within about 5% and that they were only slightly affected by the presence of a liquid film on the wetted surface.

The temperature level was determined primarily by the temperature of the cooling water at the top of the plate and the temperature gradient was dependent primarily upon the power input to the resistors at the bottom. The silver surface was prepared by metallographic polishing until a highly reflective surface was obtained with no grit marks visible at 100 $\times$ magnification in light or dark field illumination. This was followed by vapor cleaning in continuously condensing vapor of isopropanol, and finally by ion discharge cleaning at 5 kv. and 150 to 300 mamp. After the ion discharge a thin layer of nichrome alloy was evaporated onto the silver surface to lower the reflectivity and thus make interference fringes more easily visible.

The test liquid used was squalane prepared in the manner discussed by Bascom et al. (*1*), that is, purified by molecular frac-

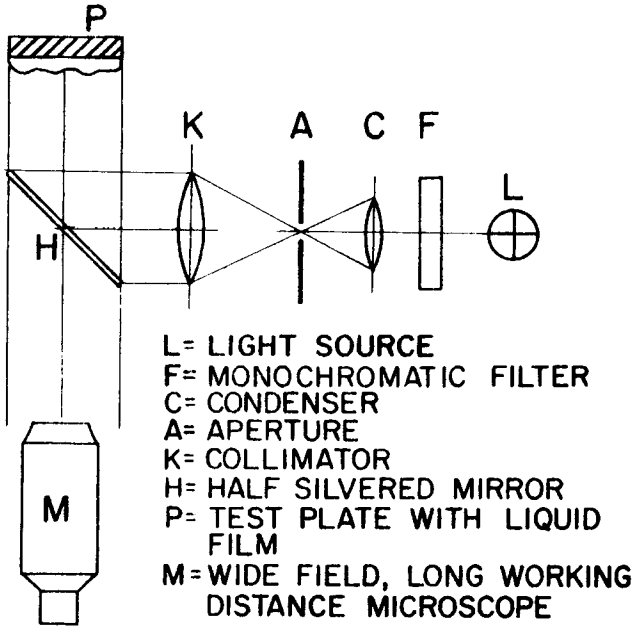

Fig. 5. Interference apparatus for observing thin films.

tionation and by a chromatographic removal of polar contaminants on Florisil.

The relevant physical properties of squalane versus temperature are presented in Figures 6 to 8. The density was measured with a Westphal balance and the kinematic viscosity with a Cannon-Fenske capillary viscometer. The surface tension was measured by the capillary method with reproducibility better than 0.2%, but the resulting average temperature coefficient of surface tension is good to only about 5%.

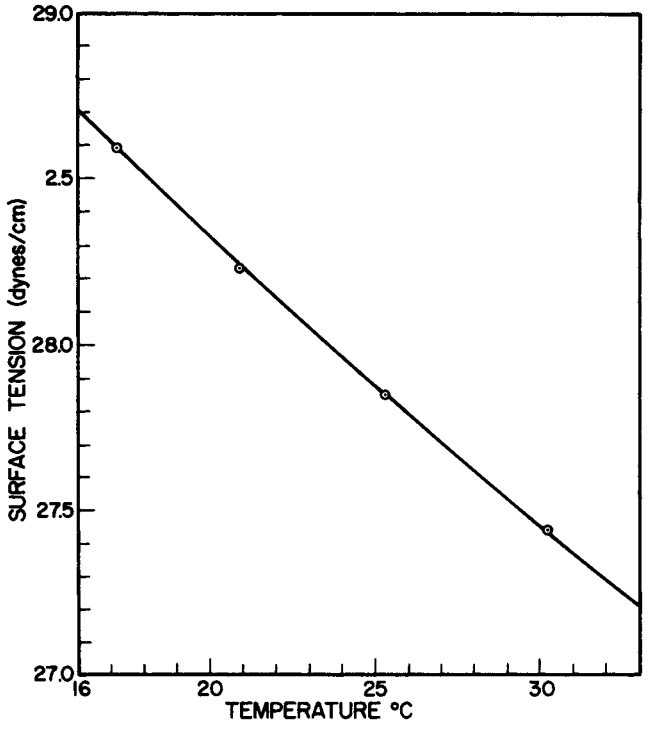

Fig. 6. Surface tension of squalane versus temperature.

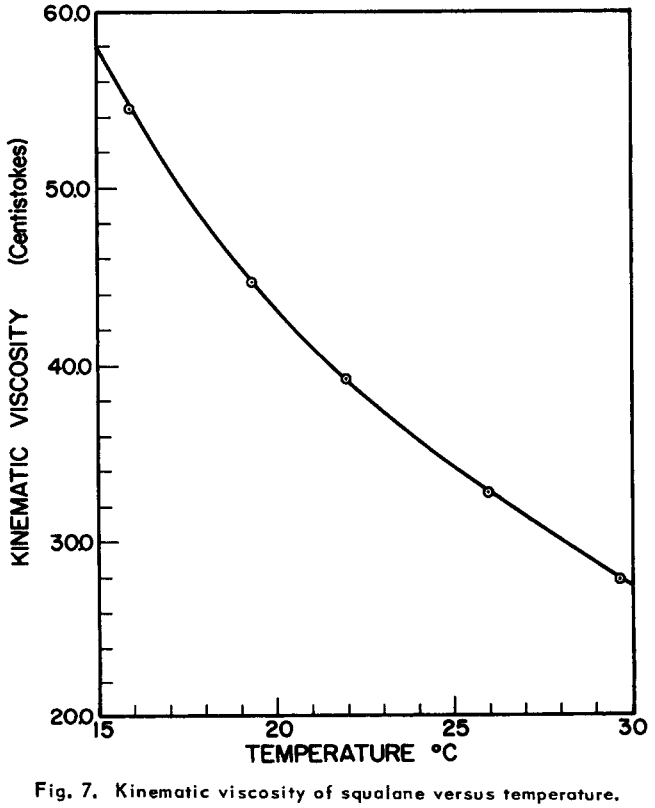

Fig. 7. Kinematic viscosity of squalane versus temperature.

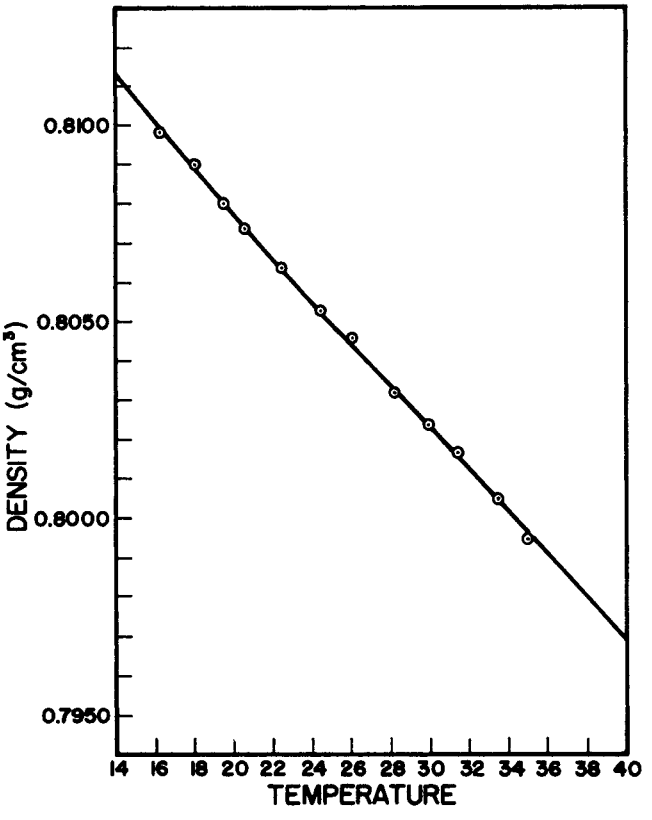

Fig. 8. Density of squalane versus temperature.

The experiments were performed in the following manner. Initially the plate was partly wetted by elevating a beaker containing squalane up around the plate until the liquid level reached about 1.5 to 2 cm. up the plate. Then the beaker was lowered slowly (about 2 mm./sec.) until the liquid surface just reached the lower end of the plate where the meniscus was maintained during the experiment.

From the initial position of the draining film the liquid would then spread upward as described below. The film would normally drain and spread evenly and no variation in thickness was observed, except near the outer edges of the plate. Thickness was measured by optical interference which gave finite increments of 0.0938 μ between interference bands.

Observations

The primary measurements were of the shapes and climbing rates of squalane films spreading upward under the influence of a surface-tension gradient. A freshly cleaned nichrome surface as described in the previous section was used in each experiment, and two series of observations were made. In the first the climbing film was allowed to spread freely to test the predictions for flow limited by the pumping capacity of the film. In the second series a horizontal surface-active barrier coating was painted across the plate to limit the height to which the film could rise. Film shape was measured when steady state was reached to test the predictions of film behavior at zero net flow. The major results of these experiments are shown in Figures 9 through 11 and discussed in the next section. It will be shown there that good agreement is obtained with the predictions. In addition, qualitative observations were made of the postulated primary film and of hydrodynamic instability during drainage and spreading. These are also discussed in the next section.

DISCUSSION OF RESULTS

Free Spreading of Squalane

In a previous section the relation

$$N_{Re} = \frac{1}{2} R^2 N_{Th} - \frac{1}{3} R^3 \qquad (18)$$

was developed to express the effects of surface-tension gradient and flow rate on film thickness. From this we

were able to show that the limiting rise rate should be given by $\frac{dZ}{d\tau} = \frac{3}{16} N_{Th}^2$ in dimensionless form, but in dimensional form

$$\frac{dz}{dt} = \frac{3}{16} \frac{\gamma^2}{\rho^2} (\nu g)^{1/3} \text{ cm./sec.} \tag{19}$$

The corresponding limiting film thickness was found to be

$$R_{\max} = N_{Th}$$

or

$$h_{\max} = \frac{\gamma}{\rho g} \tag{20}$$

The results of experiments testing these theoretical results are shown in Figures 9 and 10.

The plots of spreading distance versus time of Figure 9 show roughly a linear relationship as predicted. At the beginning of each experiment, however, the rise rate is considerably faster and a linear relation is observed only after about 4 to 6 hr. The reason for this is twofold. First each experiment was initiated by immersing the plate and then nearly immediately lowering the liquid bath before any appreciable spreading could occur. This means that the equilibrium meniscus may not have been completely established to begin with and that the initially thick film during the regular hydrodynamic draining period may allow for faster spreading than the true Marangoni film observed at longer times, for which the approximations properly hold. The second reason may be that the temperature profile was not quite linear. In fact, temperature gradients were somewhat steeper in the lower part of the plate where the spreading experiment was initiated as can be seen from sample

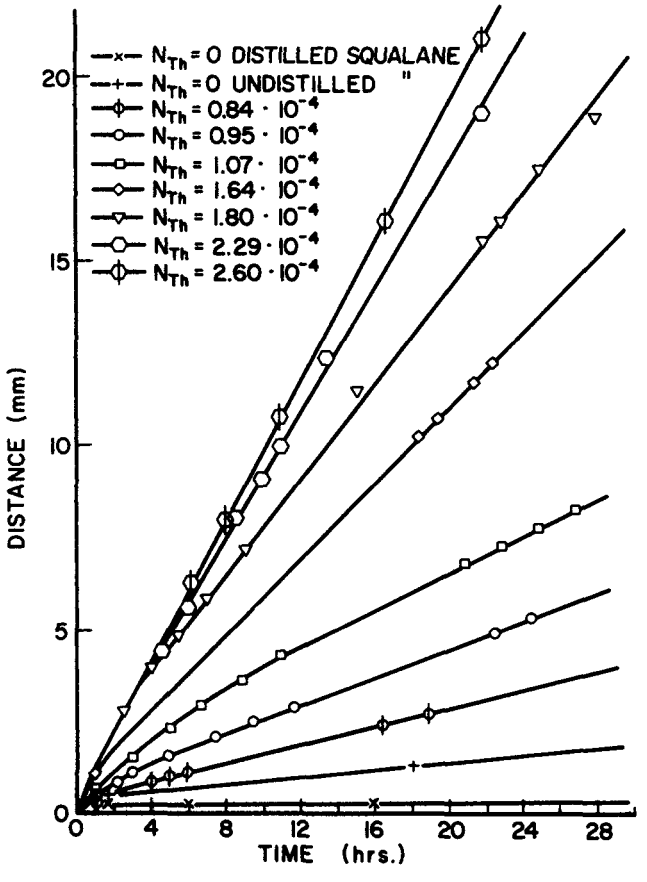

Fig. 9. Spreading of squalane as a function of Thomson number.

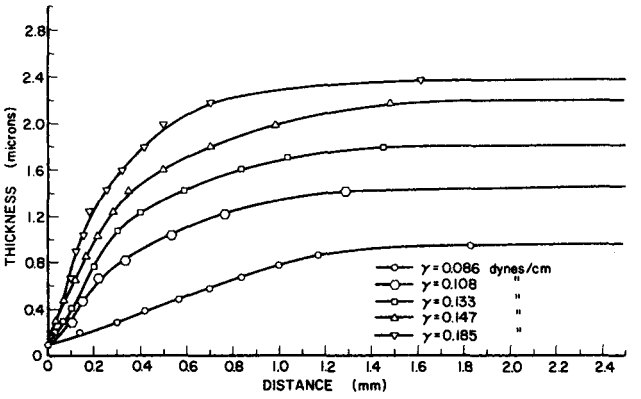

Fig. 10. Shape of film front in free spreading.

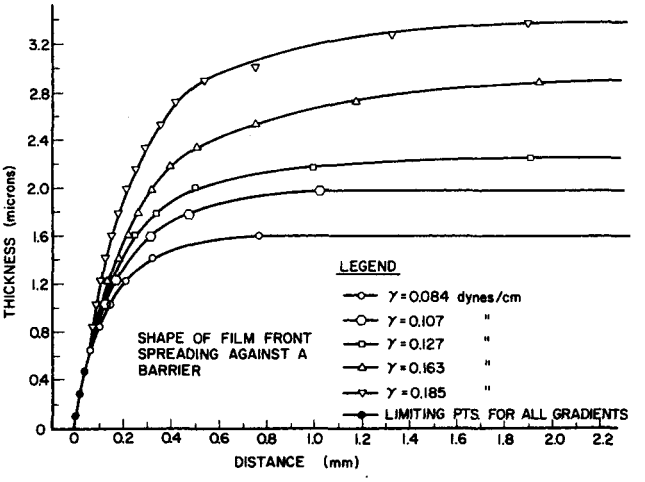

Fig. 11. Shape of film front spreading against a barrier.

temperature profiles on Figure 4*b*. These factors, together with the lower viscosity of the film due to the warmer temperatures on the lower plate surface, appear sufficient to account for the higher spreading rates in the first few hours. After this initial period all the curves show very nearly constant rise rates, which are summarized in Table 1. It should be noted that when determining the physical properties for each experiment an average temperature for the five positions is used.

From the last column we can see that the experimental rise rates are always slightly *lower* than predicted. We can determine the temperature coefficient of surface tension within better than 5% and the average temperature gradient in the plate to a maximum error of 5%. We can thus expect a maximum possible error in the predicted rise rate of about 20% and can probably do somewhat better in reality. Experiments 1, 3, 4, and 5 are well within that range, and agreement with prediction is very good. In experiment 2 the experimental rise rate is about 40% lower than predicted; this is a significant deviation. We believe that the slow experimental rise rate in this experiment was caused by slight contamination of the surface. This was chronologically the first experiment made of those presented and some initial experimental problems were encountered.

For experiments 6 and 7 the experimental rise rate does not seem to be increasing as fast with the Thomson number as theory predicts, and the discrepancy increases with increasing Thomson number. In this case it is possible that the conditions at the front of the advancing film affect the spreading rate and we do not have free spreading as assumed. This possibility is discussed further.

TABLE 1. SUMMARY OF RESULTS FOR FREE SPREADING OF SQUALANE

Exp. No.	Temp. grad. dT/dz, °C./cm.	Average temp., °C.	Thomson number $N_{Th} \times 10^4$	h_{max} [Eq. (20)], μ	h_{exp}, μ	Calc. rise rate [Eq. (19)], mm./hr.	Exp. rise rate, mm./hr.	Calc./Exp.
1	1.00	22.40	0.95	1.09	0.94	0.204	0.191	1.07
2	1.05	17.75	0.84	1.12	1.30	0.171	0.120	1.43
3	1.25	19.50	1.07	1.35	1.40	0.242	0.257	1.06
4	1.55	25.50	1.64	1.70	1.78	0.526	0.500	1.05
5	1.71	24.80	1.80	1.86	2.16	0.676	0.640	1.055
6	2.15	25.75	2.29	2.35	2.35	1.12	0.895	1.25
7	2.15	30.15	2.60	2.35	2.25	1.35	0.975	1.38

The effect of viscosity on the rise rate (through the Thomson number) can be seen from experiments 6 and 7 where the temperature gradients and hence surface-tension gradients are the same but the average temperatures are different. Viscosity varies markedly with temperature as can be seen from Figure 7 and we expect higher spreading rates for lower viscosities. Experiments 1 and 2 also demonstrate this, although less conclusively due to the possibility of contamination in 2.

Two experiments were also made at zero Thomson number (isothermally), one with distilled and one with undistilled squalane. These serve as tests of the purity of the distilled squalane used in all other experiments and of the role of surface-tension gradients. It may be seen from Figure 9 that the distilled squalane showed no detectable spreading after a short initial adjustment period. This indicates both that the squalane is effectively pure and that spreading does not occur in the absence of surface-tension gradients. The undistilled squalane, on the other hand, exhibited a finite spreading rate. This is to be expected from the results of Bascom and Singleterry (*1*) and is due to preferential evaporation of the component of lower surface tension from the upper regions of the film.

Profiles for films after free spreading of 10 to 24 hr. are shown in Figure 10. Film shapes were generally constant after 6 to 8 hr. of spreading. The increase in steady state thickness with surface-tension gradient is in agreement with prediction. Quantitative comparison between predicted and experimental terminal thickness is given in Table 1. The agreement here is within the nearest fringe order (0.0938 μ) in most cases, which is all one can expect from the experimental technique. A notable exception is experiment 5, where some difficulty was encountered in determining the highest order fringe. (As the film flattens, the fringes broaden and become interlaced, making interpretation more difficult.)

The profiles shown in Figure 10 all show a steepening of the front with increased rise rate and demonstrate a rate dependent "apparent" contact angle as predicted in a previous paper (*10*). However, at lower rates inflections in the curve fronts indicate a transition into the primary film. It appears then that the thermodynamic requirement of zero contact angle for spontaneous spreading may be satisfied by the primary film in the region below 0.0938 μ, which is the lower limit of resolution for the interference method in this system.

Visual observations of the original interferograms show a discolored or darker region rising ahead of the first fringe. This region is wider at lower flow rates and is believed by us to be the primary film, only the thickest part of which can be measured interferometrically. The position of the first-order fringe is estimated at the maximum darkness of this band. These observations are in qualitative agreement with those of Müller (*13*) for aqueous electrolytes. Müller reported a similar rapidly rising primary film and estimated its thickness as 0.05 μ. At low Thomson numbers the processes responsible for spreading of this primary film appear sufficiently rapid that they do not affect the rate of rise of the Marangoni film on which our present interest is centered. At the highest Thomson numbers used in our work, however, rate of climb of the Marangoni film may be limited by these poorly understood diffusional processes. Unfortunately it is not possible to produce higher Thomson numbers in our present equipment. We do hope to investigate system behavior at higher Thomson numbers soon.

Rise Against a Barrier—No Net Flow

The second major series of experiments was to force squalane films against a barrier of antispreading material by means of upwardly increasing surface-tension gradients. By thus stopping the spreading we produced the situation of no net flow discussed previously where we showed that for no net flow the nonzero thickness was given by $R = N_{Th}$ or

$$h = \frac{3}{2} \frac{\gamma}{\rho g} \tag{21}$$

The barrier material used was a dilute solution of perfluorooctylpolymethacrylate in Hexafluoroxylene, obtained from the Naval Research Laboratories, Washington, D.C. [This is about to be produced as an antispreading material for lubricants in bearings by the 3M Corporation (3M-Ex-706A).] The critical surface tension of this highly fluorinated compound is so low that virtually no material will spread on it.

In this experiment the squalane was allowed to rise in the normal manner under the highest temperature gradient presently attainable in the plate (2.15°C./cm.). As the film approached the barrier it slowed down from the expected rate, indicating slight diffusion of the barrier material below its assumed position. Eventually the spreading completely stopped at the barrier and now the temperature gradient could be varied at will and the limiting thickness would

TABLE 2. SUMMARY OF RESULTS FOR SQUALANE RISE AGAINST A BARRIER

Exp. No.	Temp. grad. dT/dz, °C./cm.	Average temp., °C.	$N_{Th} \times 10^4$	h_{calc} [Eq. (21)], μ	h_{exp}, μ	h_{calc}/h_{exp}
8	0.973	21.20	0.93	1.59	1.60	0.99
9	1.25	22.70	1.20	2.04	1.98	1.03
10	1.475	24.25	1.48	2.41	2.25	1.07
11	1.89	26.55	2.02	3.10	2.90	1.07
12	2.15	28.15	2.44	3.52	3.38	1.04

vary correspondingly. This thinning and thickening with surface-tension gradient was reversible.

The results of these experiments are summarized in Table 2. These results show remarkable agreement between calculated and experimental limiting film thicknesses. The uncertainty due to the factors considered before is 10% for predicting the film thickness, and all the results are within that range.

A very noteworthy feature of the results in Figure 11 is that for all the applied surface-tension gradients there is a finite concact angle which is the same for all the gradients. Furthermore, there is no hint of transition into a primary film nor can one detect any shaded area ahead of the first-order fringe in the photographs. The probable explanation for this is that the primary film does not spread over the low energy barrier material, and the contact angle is primarily determined by the equilibrium contact angle between squalane and the barrier material. It is therefore not sensitive to the applied surface tension gradient.

Observed Instabilities in Draining and Spreading Films

Several types of hydrodynamic instabilities were observed during the spreading and draining experiments. The first of these involving vertical rivulets or growing lobes has already been demonstrated and the conditions for formation analyzed (*12*). This type of instability was only observed when the draining film was still relatively thick, and was never seen in the spreading part of the film. This behavior is in agreement with the results of our earlier stability analysis (*12*).

However, after gravitational draining effects had stopped and after a constant shape for the spreading front had been established, other types of instability were observed. One of these was manifested in a somewhat jagged or lobar form of the spreading front. Some parts seemed to advance faster than others, although no parts were left far behind. This tendency was observed only for the higher spreading rates and may be explained by a slight contamination of the plate (partial monolayer) unevenly distributed.

A second type of irregularity set in after 15 to 24 hr. of spreading. About this time the film just above the normal meniscus of the test liquid in the beaker started to thin down, and within a short time had pinched off the film above it. The film thus pinched off from the bulk liquid continued to rise at the previous rate leaving a broadening region of essentially zero thickness behind it. This instability was observed only at long times for all applied surface-tension gradients and therefore did not interfere with the measurements reported in the previous sections, but it strongly indicates that rising films are unstable in a manner not hitherto considered.

CONCLUSIONS

The experimental results presented prove quite conclusively the hypothesis of Bascom et al. (*1*), that surface-tension gradients are responsible for the spontaneous spreading and maintainance of thin liquid films vertically upward on solid surfaces. The experimental results also demonstrate that the dynamics of the *bulk* film are properly described by out theoretical results.

Both the theoretical and experimental results indicate that the spreading of the film front cannot be completely described by the conventional equations of hydrodynamics alone and requires a separate physicochemical process, such as surface diffusion or multilayer adsorption for advancing the liquid front.

At low surface-tension gradients the spreading process is limited by viscous forces alone and the spreading rate depends on the supply capacity of the bulk film. At higher gradients the spreading mechanism is rate limiting and a more detailed description is necessary, taking into account the kinetics of the spreading mechanism.

Finally the experiments have shown that the Marangoni films are potentially unstable and may break up in a manner hither to not considered.

NOTATION

g = gravitational acceleration, cm./sec.^{2}
g_z = acceleration in the z direction, cm./sec.^{2}
h = film thickness, cm. or μ
$L = (\nu^2/g)^{1/3}$, reference length, cm.
$N_{Re} = h\langle v_z\rangle/\nu$, film Reynolds number or a dimensionless flow rate
$N_{Th} = (\gamma^3/\rho^3 g^2 \nu^2)^{1/3}$, Thomson number
p = pressure, dynes/sq. cm.
$R = h(g/\nu^2)^{1/3}$, dimensionless film thickness
R_d = thickness of discontinuous front (dimensionless)
$R_{\max}$ = dimensionless limiting film thickness at maximum flow rate
t = time, sec.
v_z = velocity in the z direction, cm./sec.
$\langle v_z\rangle$ = average velocity, cm./sec.
x, y, z = Cartesian coordinates, cm.
$Z = z/L$, dimensionless position along the plate
Z_d = position of the discontinuous front

Greek Letters

γ = surface-tension gradient, dynes/sq. cm.
ν = kinematic viscosity, sq. cm./sec.
μ = viscosity, g./(cm.)(sec.)
ρ = density, g./cm.^{3}
$\tau = t\nu/L^2$, dimensionless time

LITERATURE CITED

1. Bascom, W. D., R. L. Cottington, and C. R. Singleterry, *Advan. Chem. Ser.*, **43**, 355 (1964).
2. Derjaguin, B. V., and N. Zachavaeva, *Rilem Intern. Assoc. Testing Res. Labs. No. 27*, 27 (1965).
3. Derjaguin, B. V., S. V. Nerpin, and N. V. Churayev, *Rilem Intern. Assoc. Testing Res. Labs. No. 29*, 93 (1965).
4. Goldstein, S., *Proc. Royal Soc. (London)*, **A219**, *151*, 171 (1953).
5. Hardy, W. B., *Proc. Royal Soc.*, **A100**, 573 (1922).
6. Landau, L. D., and E. H. Lifshitz, "Fluid Mechanics," pp. 230–234, Pergamon Press, New York (1959).
7. Levich, V. G., "Physicochemical Hydrodynamics," Prentice-Hall, Englewood Cliffs, N. J. (1962).
8. Lightfoot, E. N., and V. Ludviksson, *J. Electrochem. Soc.*, **113**, 1325 (1966).
9. Lightfoot, E. N., R. J. Sanchez-Palma, and D. O. Edwards, "New Chemical Engineering Separations Techniques," H. M. Schoen, ed., p. 83, Interscience, New York (1962).
10. Ludviksson, V., and E. N. Lightfoot, *AIChE J.*, **14**, No. 4, 674 (1968).
11. Ludviksson, V., Ph.D. thesis, Univ. Wisconsin, Madison (May 1968).
12. ———, and E. N. Lightfoot, *AIChE J.*, **14**, No. 4, 620 (1968).
13. Müller, R. H., *Univ. California, Berkeley, UCRL-16626, AEC Contract No. N-7405-Eng-48* (Dec. 1965).
14. ———, *J. Opt. Soc. Am.*, **54**, 419, 1964.
15. ———, *Univ. California, Berkeley UCRL-10963, AEC Contract No. W-7405-Eng-48* (July 1963).
16. Pearson, J. R. A., *J. Fluid. Mech.*, **4**, 489–500 (1958).
17. Scriven, L. E., and C. V. Sternling, *ibid.*, **19**, 321–340 (1963).
18. Tallmadge, J. A., and Chaim Gutfinger, *Ind. Eng. Chem.*, **59**(11), 18–34 (1967).
19. Thomson, J., *Phil. Mag.*, **10** (4th Ser.), 330 (1855).
20. Tobolsky, S., "Surface Microtopography," Interscience, New York (1960).
21. Will, F. G., *J. Electrochem. Soc.*, **110**, 145 (1963).
22. *Ibid.*, 152–160 (1963).

Manuscript received October 10, 1968; revision received August 4, 1969; paper accepted August 7, 1969.